European Congress on Computational Methods in Applied Sciences and Engineering
ECCOMAS 2004
P. Neittaanmäki, T. Rossi, K. Majava, and O. Pironneau (eds.)
R. Owen and M. Mikkola (assoc. eds.)
Jyväskylä, 24–28 July 2004

COMPARISON BETWEEN TWO COHESIVE-ZONE MODELS FOR THE ANALYSIS OF INTERFACE DEBONDING

Giulio Alfano[†], Silvio de Barros[⋆], Laurent Champaney[⋆] and Nunziante Valoroso[‡]

[†]Dipartimento di Scienza delle Costruzioni
Università di Napoli Federico II
Via Claudio 21, 80125 Napoli, Italy
e-mail: gialfano@unina.it

[⋆] Laboratoire d'Etudes Mécaniques des Assemblages
Université de Versailles Saint-Quentin-en-Yvelynes
45, Avenue des Etats Unis, 78035 Versailles Cedex, France
e-mail: laurent.champaney@meca.uvsq.fr

[‡] Istituto per le Tecnologie della Costruzione
Consiglio Nazionale delle Ricerche
Viale Marx 15, 00137 Roma, Italy
e-mail: nunziante.valoroso@itc.cnr.it

Key words: cohesive-zone, interfaces, debonding, damage, mixed-mode.

Abstract. *Two cohesive-zone models, one developed by Valoroso & Champaney and the other initially proposed by Crisfield and co-workers and later modified by Alfano & Crisfield, are used for studying a set of delamination problems.*

Both models consider irreversible damage of the interface and account for mixed-mode debonding by satisfying a generalised ellipse-like interaction criterion.

In this paper a comparative analysis of the two models is carried out; results are presented and discussed for numerical simulations referring to both single-mode and mixed-mode situations.

1 INTRODUCTION

Cohesive-zone models have been extensively used for the non-linear incremental analysis of interface debonding in the last years [1–12].

Unlike other methods that are directly based on fracture mechanics, they do not require the presence of an initial crack, can be more easily coupled with other material and geometric nonlinearities and allow for efficient implementations in a finite element setting via interface elements. Nevertheless, their use is often limited by the requirement for a very refined mesh around the process zone and because of the strongly nonlinear structural response, which might be difficult to follow even by using sophisticated path-following techniques [13].

In this paper a comparison between two cohesive-zone models is presented. Both of them consider irreversible damage and, for the mixed-mode case, satisfy a generalized ellipse-like fracture criterion [14].

The first one, developed by Valoroso and Champaney in [15, 16], is derived within a damage mechanics framework and is based upon a quite general formulation that allows to recover several earlier interface models proposed in the literature. In particular, in the present work two cases are considered that, for the pure-mode situation, result in a polynomial [1, 17] and in an exponential [15, 16] traction-displacement jump relationship.

The second model studied, developed by Crisfield and his coworkers in [8] and later modified by Alfano and Crisfield in [18], specialises to bilinear interface relationships for pure-mode cases. The model was initially formulated in [8] by means of an explicit mixed-mode relationship between the relative-dispalcement vector and the traction on the interface, but it has then been derived in [18] in the framework of damage mechanics. It is shown, briefly in the paper and more in detail in [16], that this model can be derived as a specialization of the one described by Valoroso and Champaney.

The outline of the paper is as follows. In Section 2 a brief introduction of both cohesive-zone models is given while Sections 2.1 and 2.2 describe the two models. In Section 3 the results of the numerical simulations of four delamination problems are presented. The first two cases involve mode-I crack propagation, while mixed-mode debonding is considered in the third and fourth example. Some conclusions are finally drawn in Section 4.

2 INTERFACE MODEL

In the cohesive-zone approach the description of a state of damage along an interface relies upon the definition of a traction-separation law incorporating the dependence of the surface tractions on the corresponding displacement discontinuities $[\mathbf{u}] = \mathbf{u}^+ - \mathbf{u}^-$ and the damage criterion to be met for the cohesive process zone to grow and the crack to advance. In the simplest one-dimensional case the damage onset and decohesion propagation conditions only involve the single-mode displacement or energy release rate component; on the contrary, when considering the mixed-mode case these conditions have to properly account for the interaction of the pure-mode contributions.

In this last case the work of separation per unit fracture surface area

$$G_T = G_I + G_{II} \tag{1}$$

does actually results from the interplay of the I and II pure-mode contributions, that are not independent in that they evolve together as a consequence of the interaction of the traction-displacement jump relationships in the two directions.

In what follows we shall briefly discuss the constituive relationships adopted in this paper by directly considering the mixed-mode situation. A more exhaustive presentation of the constitutive models can be found elsewhere [8, 15, 16, 18].

2.1 Model A (Valoroso & Champaney, 2004)

Consider the following form of the stored energy function [15, 16]:

$$\psi([\mathbf{u}], D) = \frac{1}{2}(1-D)\left[k_n^+ \langle [u_n] \rangle_+^2 + k_s [u_s]^2\right] + \frac{1}{2} k_n^- \langle [u_n] \rangle_-^2 \tag{2}$$

where $D \in [0,1]$ is the scalar damage variable and $[u_n]$ and $[u_s]$ denote the normal and sliding components of the displacement jump vector $[\mathbf{u}]$. In the above relationship k_n^+, k_n^-, k_s are the undamaged interface stiffnesses while the symbols $\langle \cdot \rangle_+$ and $\langle \cdot \rangle_-$ stand for the positive and negative part of the argument $\langle \cdot \rangle$, defined as $\langle x \rangle_\pm = 1/2(x \pm |x|)$.

The constitutive equations for the interface traction vector and the work-conjugate of the damage variable follow from the classical thermodynamic argument as [19]:

$$\begin{aligned} \mathbf{t} &= \frac{\partial \psi}{\partial [\mathbf{u}]} = (1-D)\left[k_n^+ \langle [u_n] \rangle_+ \mathbf{n} + k_s [u_s] \mathbf{s}\right] + k_n^- \langle [u_n] \rangle_- \mathbf{n} \\ Y_m &= -\frac{\partial \psi}{\partial D} = Y_I + Y_{II} \end{aligned} \tag{3}$$

where $\mathbf{n}$ is the outward unit normal, $\mathbf{s}$ is the unit tangent vector to the interface, the subscript m stands for mixed-mode and the pure-mode energy release rates Y_I and Y_{II} are given by:

$$Y_I = \frac{1}{2} k_n^+ \langle [u_n] \rangle_+^2 \,; \qquad\qquad Y_{II} = \frac{1}{2} k_s [u_s]^2 \tag{4}$$

Based on (3) the mixed-mode energy release rate Y_m can be expressed as:

$$Y_m = \frac{1}{2} k_n^+ \delta^2 \tag{5}$$

where δ is the equivalent opening displacement parameter:

$$\delta = \left(\langle [u_n] \rangle_+^2 + \alpha^2 [u_s]^2 \right)^{1/2} \tag{6}$$

for

$$\alpha = \sqrt{\frac{k_s}{k_n^+}} \tag{7}$$

A mode mixity parameter $\boldsymbol{\beta}$ can thus be defined as:

$$\boldsymbol{\beta} = \alpha \tan(\varphi) \tag{8}$$

φ being the loading angle:

$$\varphi = \arctan\left[\frac{[u_s]}{\langle [u_n] \rangle_+}\right] \in [0, +\pi/2] \tag{9}$$

Accordingly, the pure-mode contributions (4) to the energy release rate (5) turn out to be:

$$\begin{aligned} Y_I &= \frac{1}{1+\boldsymbol{\beta}^2} Y_m \\ Y_{II} &= \frac{\boldsymbol{\beta}^2}{1+\boldsymbol{\beta}^2} Y_m \end{aligned} \tag{10}$$

By ruling out the penalty term accounting for non-interpenetration, the cohesive relationship $(3)_1$ can be equivalently expressed as:

$$t_\delta = (1-D) k_n^+ \delta \tag{11}$$

where t_δ is the equivalent traction:

$$t_\delta = \left(t_n^2 + \frac{1}{\alpha^2} t_s^2\right)^{1/2} \tag{12}$$

and

$$t_n = \langle \mathbf{t} \cdot \mathbf{n} \rangle_+ = \frac{1}{(1+\boldsymbol{\beta}^2)^{1/2}} t_\delta; \qquad t_s = \mathbf{t} \cdot \mathbf{s} = \frac{\alpha \boldsymbol{\beta}}{(1+\boldsymbol{\beta}^2)^{1/2}} t_\delta \tag{13}$$

are the normal and sliding traction components.

By appealing to maximum damage dissipation we are lead to the normal evolution equation:

$$\dot{D} = \dot{\gamma} \frac{\partial \boldsymbol{\phi}_m}{\partial Y_m} \tag{14}$$

for the damage criterion:

$$\boldsymbol{\phi}_m = Y_m - Y_m^* \leq 0 \tag{15}$$

where Y_m^* represents the mixed-mode critical energy release rate.

The damage model is characterized by the relationship between the critical damage driving force Y_m^* and D. For the case at hand this can be expressed in the form:

$$\begin{cases} Y_m^* = Y_{mo} & \text{if } D = 0 \\ Y_m^* = F_m(D) & \text{if } D \in]0,1[\\ Y_m^* = \max\limits_{\tau \le t} Y_m(\tau) & \text{if } D = 1 \end{cases} \tag{16}$$

where, owing to the irreversibility of damage, the function F_m has to be taken positive, monotone non-decreasing and vanishing on $\Re_0^-$.

The damage model requires two parameters, Y_{mo} and Y_{mf}, which can be computed based on single-mode parameters that enter the adopted criteria for damage onset and decohesion propagation. In particular, assuming that initiation of damage can be predicted using an interaction criterion of the type:

$$\left(\frac{Y_I}{G_{oI}}\right)^{\alpha_1} + \left(\frac{Y_{II}}{G_{oII}}\right)^{\alpha_2} - 1 = 0 \tag{17}$$

where G_{oI} and G_{oII} are the initial pure-mode damage thresholds, for a given loading angle (9) the initial mixed-mode threshold Y_{mo} is computed from (17) that, on account of (10), can be given the form:

$$c_I \left(Y_m\right)^{\alpha_1} + c_{II} \left(Y_m\right)^{\alpha_2} - 1 = 0 \tag{18}$$

for

$$c_I = \left[\frac{1}{(1+\boldsymbol{\beta}^2)G_{oI}}\right]^{\alpha_1}; \quad c_{II} = \left[\frac{\boldsymbol{\beta}^2}{(1+\boldsymbol{\beta}^2)G_{oII}}\right]^{\alpha_2} \tag{19}$$

For $\alpha_2 = \alpha_1$ one has then from equation (18):

$$Y_{mo} = \frac{(1+\boldsymbol{\beta}^2)G_{oI}G_{oII}}{\left[(G_{oII})^{\alpha_1} + (\boldsymbol{\beta}^2 G_{oI})^{\alpha_1}\right]^{1/\alpha_1}} \tag{20}$$

whence the pure-mode threshold energies G_{oI} and G_{oII} are recovered in the limit as $\varphi \to 0$ and $\varphi \to \pi/2$ respectively.

Following reference [14], the adopted propagation condition, stemming from one of the most widely used criteria to predict the propagation of delamination in composites, is a generalized ellipse-like criterion

$$\left(\frac{G_I}{G_{cI}}\right)^{\beta_1} + \left(\frac{G_{II}}{G_{cII}}\right)^{\beta_2} - 1 = 0 \tag{21}$$

where the mode I and mode II released energies are given by:

$$G_i = \int_0^{+\infty} Y_i \dot{D} \mathrm{d}t\,; \qquad i \in \{I, II\} \tag{22}$$

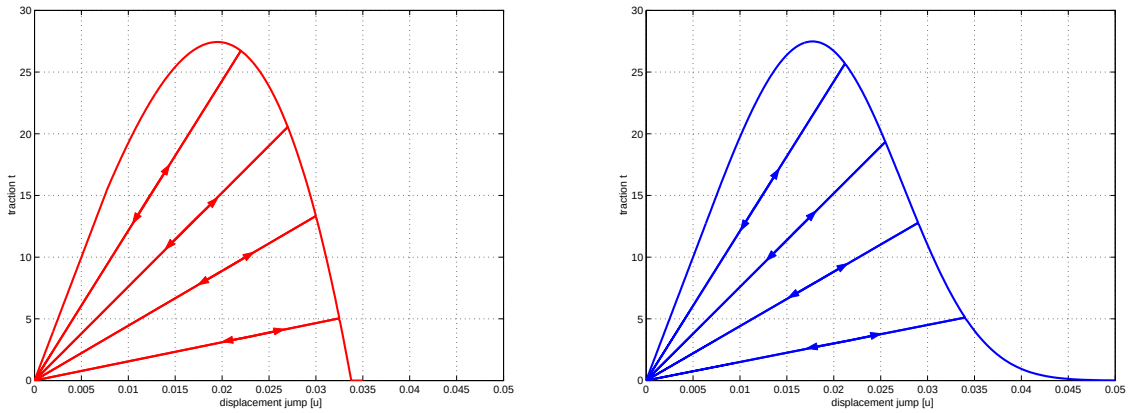

Figure 1: Pure-mode traction-separation relationships for model A.

From (10) it follows that, for proportional loading, the ratio between G_{II} and G_I is constant and equals $\boldsymbol{\beta}^2$; accordingly, from (21) one has the nonlinear equation:

$$d_I \left(G_T\right)^{\beta_1} + d_{II} \left(G_T\right)^{\beta_2} - 1 = 0 \tag{23}$$

where G_T is defined by (1) and the coefficients d_I and d_{II} have the same expression as in (19) except for G_{oI} and G_{oII} being replaced by G_{cI} and G_{cII}.

For $\beta_2 = \beta_1$ the propagation of decohesion then takes place for:

$$G_T = \frac{(1+\boldsymbol{\beta}^2) G_{cI} G_{cII}}{\left[(G_{cII})^{\beta_1} + (\boldsymbol{\beta}^2 G_{cI})^{\beta_1}\right]^{1/\beta_1}} \tag{24}$$

where G_T is computed as the total work of separation:

$$G_T = \int_0^{+\infty} Y_m^* \dot{D} \, \mathrm{d}t \tag{25}$$

whose expression depends upon that of the function F_m defining the critical damage-driving force in the range $D \in]0,1[$. Taking for F_m one of the forms [15, 17]:

$$F_m(D) = \begin{cases} Y_{mo} + (Y_{mf} - Y_{mo}) D^{1/N} \\ Y_{mo} + (Y_{mf} - Y_{mo}) [-\log(1-D)]^N \end{cases} \tag{26}$$

for $N > 0$ (not necessarily integer), upon comparison of (24) and (25) the expression of the characteristic value of the mixed-mode energy release rate Y_{mf} is then obtained as:

$$Y_{mf} = \begin{cases} \dfrac{1}{N}[(N+1) G_T - Y_{mo}] \\ Y_{mo} + \dfrac{1}{\boldsymbol{\Gamma}(N+1)} [G_T - Y_{mo}] \end{cases} \tag{27}$$

$\boldsymbol{\Gamma}$ being the Gamma function [20]. The pure-mode traction-separation laws corresponding to $(26)_1$ (Allix-Ladevèze model) and $(26)_2$ (exponential model) are depicted in Figure 1.

2.2 Model B (Crisfield et al., 1998; Alfano & Crisfield, 2001)

The cohesive-zone model initially proposed in [8] and later modified in [18] can be formulated in an explicit way by directly defining the non-linear interface relationship between the displacement jump $[\mathbf{u}]$ and the interface traction $\mathbf{t}$. To this end, the following parameter is introduced:

$$\tilde{\gamma} = \left[\left(\frac{Y_I}{G_{oI}} \right)^{\mu} + \left(\frac{Y_{II}}{G_{oII}} \right)^{\mu} \right]^{\frac{1}{\mu}} - 1 \tag{28}$$

where the scalar μ is a material parameter and Y_I and Y_{II} are defined as in (4).

The existence of two initial, pure-mode damage thresholds G_{oI} and G_{oII} is again assumed; furthermore, a parameter η is introduced in the model and the following hypothesis is made [18]:

$$\frac{G_{oI}}{G_{cI}} = \frac{G_{oII}}{G_{cII}} = 1 - \eta \tag{29}$$

with G_{cI} and G_{cII} being the pure-mode fracture energies.

Denoting by γ the maximum value of $\tilde{\gamma}$ which has been attained over the previous history at the point at hand

$$\gamma = \max_{\tau \leq t} \tilde{\gamma}, \tag{30}$$

the explicit interface relationship is then written as follows:

$$\mathbf{t} = \begin{cases} \mathbf{K}[\mathbf{u}] & \text{if } \gamma \leq 0 \\ (\mathbf{I} - D\mathbf{C})\, \mathbf{K}[\mathbf{u}] & \text{if } \gamma > 0 \end{cases} \tag{31}$$

where $\mathbf{K} = \text{diag}[k_n, k_s]$, with k_n and k_s representing the normal and tangential initial stiffnesses, $\mathbf{C} = \text{diag}[\,\mathrm{h}\,([u_n]), 1]$, with $\mathrm{h}\,(x)$ being the Heaviside function

$$\mathrm{h}\,(x) = 1 \quad \text{if } x \geq 0 \quad \text{and} \quad \mathrm{h}\,(x) = 0 \quad \text{if } x < 0, \tag{32}$$

$\mathbf{I}$ is the identity tensor and the damage parameter D is defined as:

$$D = \min \left\{ 1, \frac{1}{\eta} \left(\frac{\gamma}{1+\gamma} \right) \right\} \tag{33}$$

Notice that the matrix $\mathbf{C}$ plays a role when $[u_n] < 0$, in which case mode I does not interact with mode II and the simple relationship $t_n = k_n\,[u_n]$ is obtained for mode I, whereby k_n represents a penalty stiffness used to prevent material overlapping.

As shown in [18], for a fixed mode-ratio the fracture criterion (21) is fulfilled for the present model by taking $\beta_1 = \beta_2 = \mu/2$, where in this explicit formulaton the mode-I and mode-II released energies are given by:

$$G_I = \int_0^{+\infty} t_n\,[\dot{u_n}]\,\mathrm{d}\,t \qquad\qquad G_{II} = \int_0^{+\infty} t_s\,[\dot{u_s}]\,\mathrm{d}\,t \tag{34}$$

The set of input parameters for the model, as described by equations (28)-(33), is represented by the fracture energies G_{cI} and G_{cII}, the damage threshold energies G_{oI} and G_{oII} and the stiffnesses k_n and k_s. In the pure-mode cases, the model specialises to the piecewise linear, pure-mode laws depicted in figure 2. With reference to this figure, G_{oI} and G_{oII} represent the specific work done by the tractions in modes I and II, respectively corresponding to the relative displacements values $[u_{no}]$ and $[u_{so}]$ while t_{no} and t_{so} are the values of the traction components at $[u_{no}]$ and $[u_{so}]$.

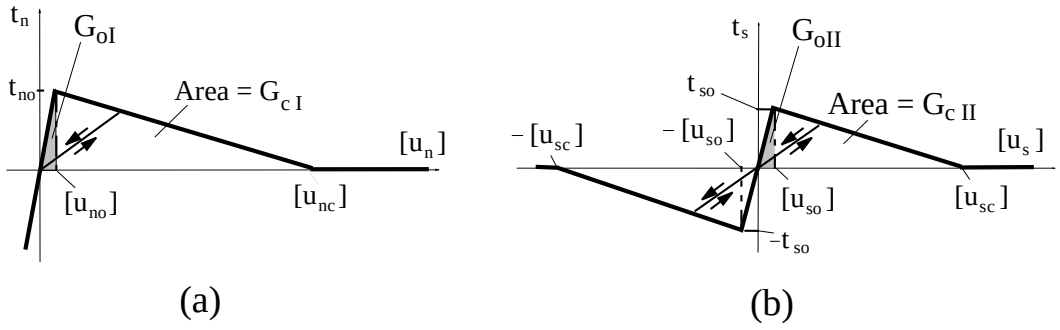

Figure 2: Bilinear pure-mode interface laws for Crisfield model: (a) mode I; (b) mode II.

The following relationships clearly hold:

$$G_{oI} = \frac{1}{2} t_{no}\,[u_{no}]; \qquad G_{oII} = \frac{1}{2} t_{so}\,[u_{so}]; \qquad k_n = \frac{t_{no}}{[u_{no}]}; \qquad k_s = \frac{t_{so}}{[u_{so}]} \tag{35}$$

whereby the model can equivalently be described in terms of another set of input parameters, namely $\{G_{cI},\, G_{cII},\, t_{no},\, t_{co},\, [u_{no}],\, [u_{so}]\}$.

The values of the relative-displacement components at which damage has fully developed in the pure-mode cases have been denoted by $[u_{nc}]$ and $[u_{sc}]$ in figure 2 and are related to the other parameters by the relationships $[u_{nc}] = 2\,G_{cI}/t_{no}$ and $[u_{sc}] = 2\,G_{cII}/t_{so}$.

It is worth noticing that, in terms of relative-displacement components, the assumption (29) is equivalent to:

$$\frac{[u_{no}]}{[u_{nc}]} = \frac{[u_{so}]}{[u_{sc}]} = 1 - \eta \tag{36}$$

while variable $\tilde{\gamma}$ introduced in equation (28) can be given the expression:

$$\tilde{\gamma} = \left[\left(\frac{\langle [u_n] \rangle_+}{[u_{no}]} \right)^{\mu} + \left(\frac{|[u_s]|}{[u_{so}]} \right)^{\mu} \right]^{\frac{1}{\mu}} - 1 \tag{37}$$

2.2.1 Damage-mechanics formulation

The Crisfield model has been briefly described so far by means of an explicit approach analogous to that initially proposed in [8]. The same model has then been reformulated in [18] within the more general framework of damage mechanics starting from the following expression of the free energy potential:

$$\tilde{\psi}([\mathbf{u}], D_n, D_s) = \frac{1}{2}(1 - D_n)k_n\langle[u_n]\rangle_+^2 + \frac{1}{2}(1 - D_s)k_s[u_s]^2 + \frac{1}{2}k_n\langle[u_n]\rangle_-^2 \tag{38}$$

Having introduced, at least initially, two damage parameters D_n and D_s, differentiation of the free energy leads to the definition of two damage-driving forces Y_I and Y_{II}, respectively conjugate to D_n and D_s, instead of the variable Y_m defined as in (3), see Section 2.1. Accordingly, the damage function introduced in [18] separately depends upon Y_I and Y_{II} and, in order to ultimately have only one damage parameter, a damage evolution law of non-associative type was used.

However, it is possible to show that an equivalent damage-mechanics formulation of Crisfield model can also be obtained as a specialization of the model described in Section 2.1 model by setting $k_n^+ = k_n^- = k_n$ in (2), $\alpha_1 = \mu/2$ in equation (20) and by making the following choice for the damage function F_m:

$$F_m(D) = \frac{(1 + \beta^2)\,(1 - \eta)}{(1 - \eta\, D)^2 \left[\left(\dfrac{1}{G_{cI}}\right)^{\mu/2} + \left(\dfrac{\beta^2}{G_{cII}}\right)^{\mu/2}\right]^{2/\mu}} \tag{39}$$

see also [16] for further details.

3 NUMERICAL EXAMPLES

The interface models briefly described in the previous sections have been implemented as a part of the finite element codes CAST3M [21], developed by the CEA (Commisariat à l'Energie Atomique), and LUSAS [22]. For the numerical examples described in this section use has been made of 8-noded plane strain quadrilaterals for the bulk material and 6-noded interface elements for which Newton-Cotes integration is adopted. Computations have been carried out by using a varying step size and a local-control-based arc-length algorithm as discussed in [13].

In order to make possible a comparison of the different models, we consider for all of them the same initial (undamaged) interface stiffnesses while the remaining material parameters are tuned in a way to obtain equal values for the fracture energy and the local peak stress. In particular, since the peak stress is only indirectly defined in the Allix-Ladevèze and exponential models discussed in Section 2.1, for these models the exponents N have been adjusted in order to get a value of the maximum traction approximately equal to the one corresponding to the beginning of the softening branch of the bi-linear traction-relative displacement relationship referred to in Section 2.2.

3.1 DCB test

As a first example we consider the Double Cantilever Beam (DCB) test. Loading is simulated via displacement control and the dimensions of the specimen are similar to those adopted for typycal experimental tests used for measuring the mode-I fracture energy, see Figure 3. The material data set for this problem is given in Table 1.

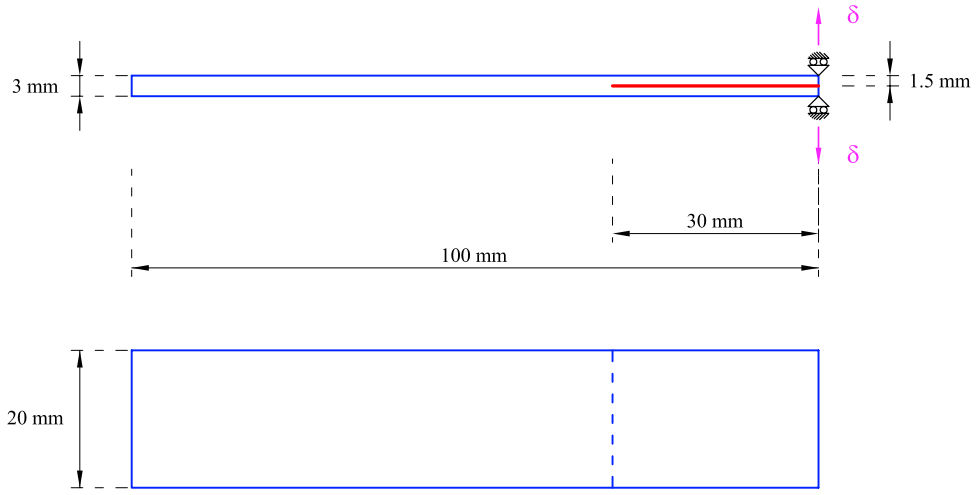

Figure 3: DCB test. Model problem.

Bulk material	$E = 70$ (GPa)	$\nu = 0.3$			
Interface parameters	k_n (N/mm^3)	G_o (N/mm)	G_c (N/mm)	t_o (N/mm^3)	N
Allix-Ladevèze model	1.000E+04	1.125E-02	5.000E-01	3.002E+01	1.980E-01
Exponential model	1.000E+04	1.125E-02	5.000E-01	3.004E+01	1.720E+00
Crisfield model	1.000E+04	4.500E-02	5.000E-01	3.000E+01	-

Table 1: DCB test. Material data.

The computed load-deflection curves, all referring to a regular mesh made of 284×4 continuum elements and 280 interface elements, are depicted in Figure 4. No substantial difference appears between the responses obtained with the three different models, that are practically coincident owing to the very refined mesh used for the simulation and to the relatively small stiffness of the sample.

3.2 Compact specimen test

The second example concerns a compact specimen obtained by increasing the thickness of the arms of the DCB from $1.5mm$ to $50mm$.

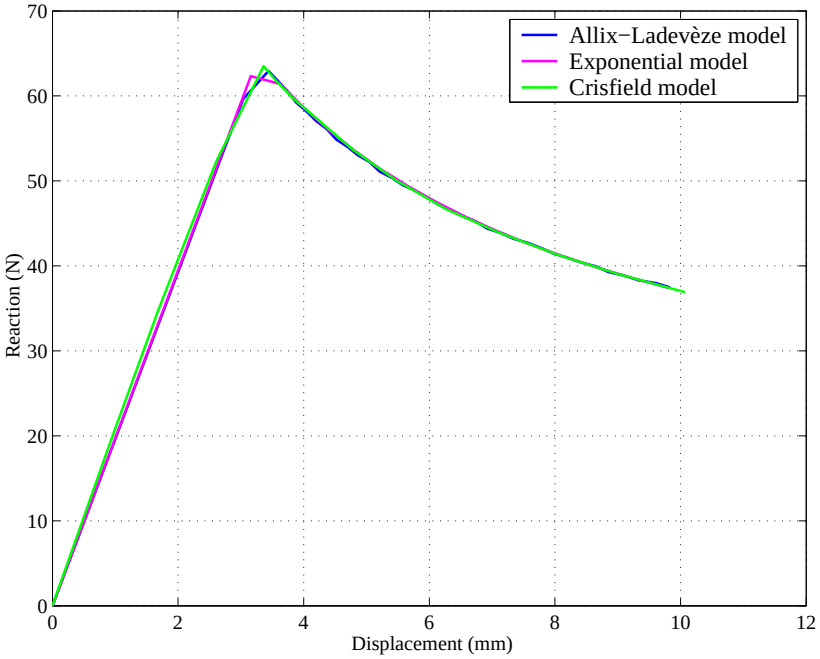

Figure 4: DCB test. Computed load-deflection curves.

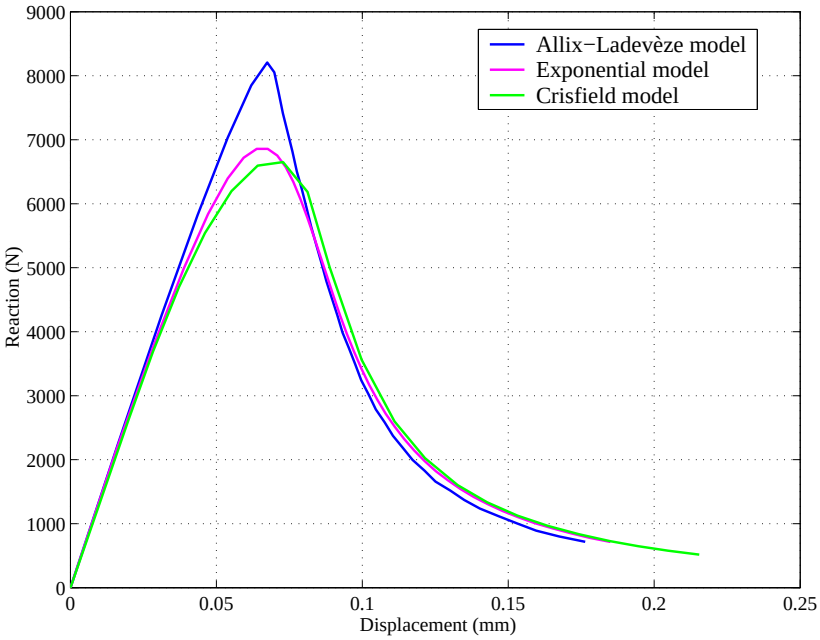

Figure 5: Compact specimen test. Computed load-deflection curves.

The material data set for this example is the same as in Table 1 except for the elastic moduli of the bulk material that have been changed to $E = 210GPa$ and $\nu = 0.2$. The computed results have been obtained using a regular mesh made of 78×16 continuum elements and 70 interface elements.

Owing to the increased stiffness of the specimen the difference between the load-deflection curves obtained for the different interface models, see Figure 5, becomes here more apparent. In particular, for this problem the Allix-Ladevèze model yields an increase in the peak load of about 20% compared to the exponential and bi-linear models.

As alredy pointed out in [23], this fact shows that, for a very stiff sample, the shape of the traction-separation law may significantly influence the size of the process zone that in this case can have a length comparable to the dimensions of the sample itself.

3.3 Mixed-mode flexure test (MMF)

The third example refers to the mixed-mode flexure test originally proposed in [24]. The geometry of the specimen is depicted in Figure 6 and the material data set is given in Table 2. In particular, the parameters α_1 and β_1 governing the shape of the damage onset and failure loci have both been taken equal to 2.0.

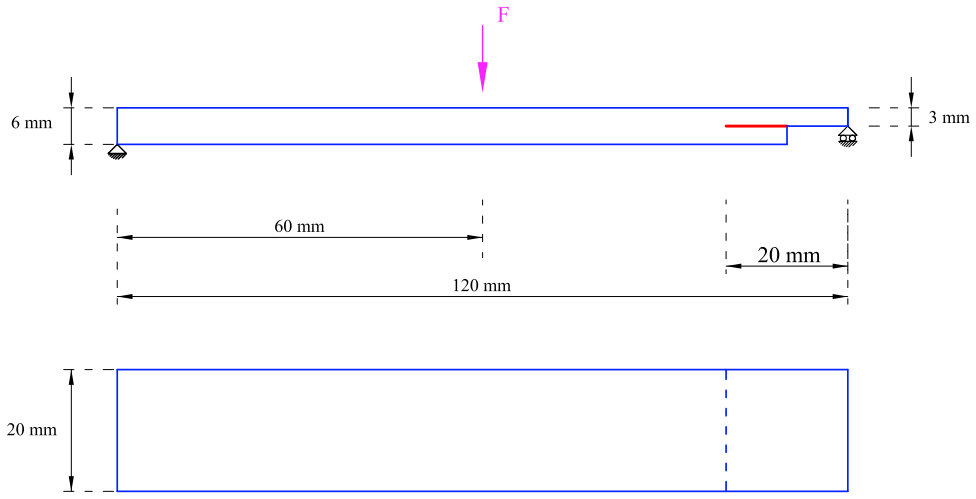

Figure 6: MMF test. Model problem.

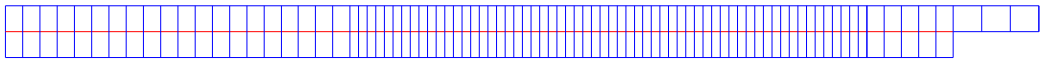

Figure 7: MMF test. FE mesh.

Bulk material	$E = 70$ (GPa)	$\nu = 0.3$			
Interface parameters	k_n (N/mm^3)	G_{oI} (N/mm)	G_{cI} (N/mm)	t_{no} (N/mm^3)	N
Allix-Ladevèze model	1.000E+04	2.813E-03	1.250E-01	1.501E+01	1.975E-01
Exponential model	1.000E+04	2.813E-03	1.250E-01	1.502E+01	1.696E+00
Crisfield model	1.000E+04	1.125E-02	1.250E-01	1.500E+01	-
	k_s (N/mm^3)	G_{oII} (N/mm)	G_{cII} (N/mm)	t_{so} (N/mm^3)	α_1, β_1
Allix-Ladevèze model	1.000E+04	1.125E-02	5.000E-01	3.002E+01	2.000E+00
Exponential model	1.000E+04	1.125E-02	5.000E-01	3.004E+01	2.000E+00
Crisfield model	1.000E+04	4.500E-02	5.000E-01	3.000E+01	2.000E+00

Table 2: MMF test. Material data.

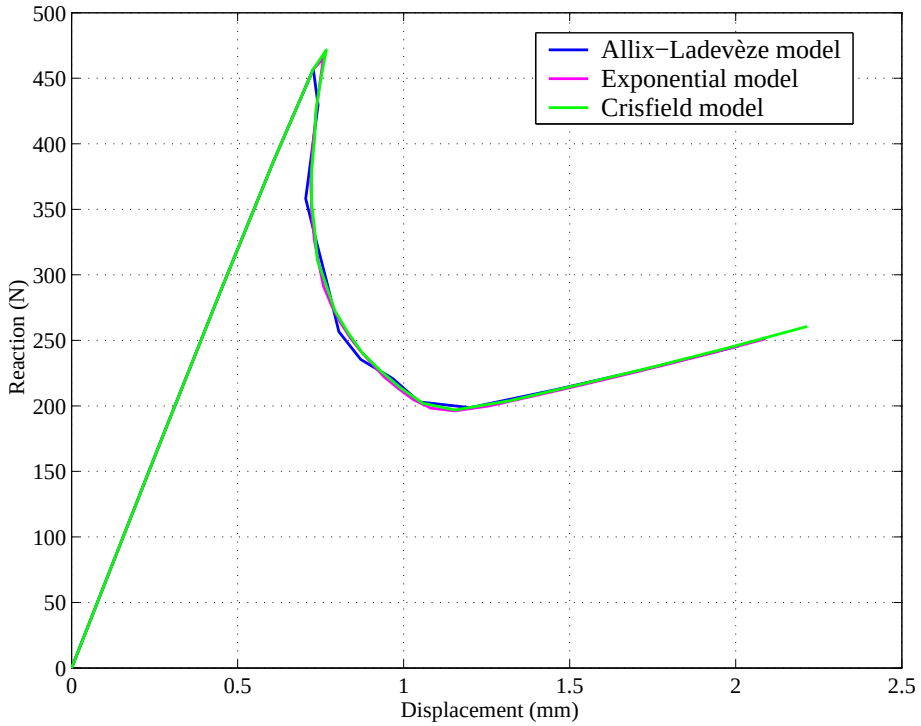

Figure 8: MMF test. Computed load-deflection curves.

The load-deflection curves, computed by using the FE mesh given in Figure 7, are shown in figure 8. It can be observed that the three solution are in fairly good agreement.

This substantially confirms what is found for the DCB test, i.e. that for a relatively flexible specimen use of a sufficiently fine mesh and of an adequate time increment size gives results that are quite insensitive with respect to the detail of the different traction-separation laws.

3.4 Mixed-mode thick specimen test (MMT)

The fourth problem analyzed is that of a thick specimen under mixed-mode loading, see Figure 9, for which the material data set is the same as in the previous example.

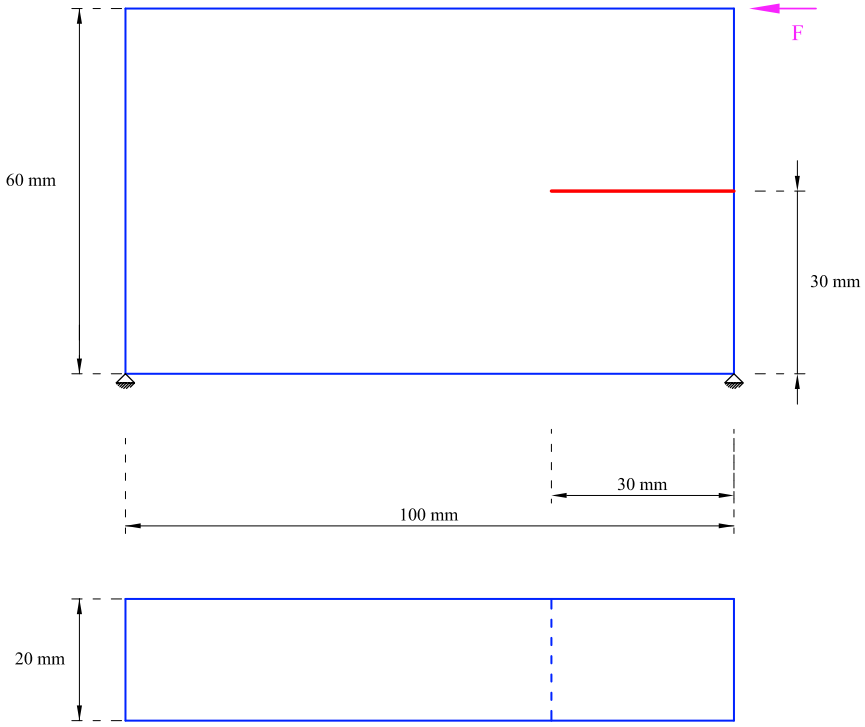

Figure 9: MMT test. Model problem.

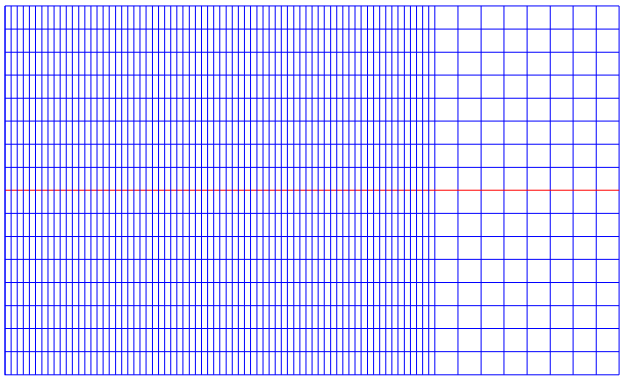

Figure 10: MMT test. FE mesh.

Loading is simulated via a point load applied to the upper arm of the sample; stress transfer to the lower arm then takes place through normal (mode I) and sliding (mode II) tractions along the interface.

The load-deflection curves shown in Figure 11 have been obtained using the FE mesh sketched in Figure 10, consisting of 78×16 continuum elements and 70 interface elements.

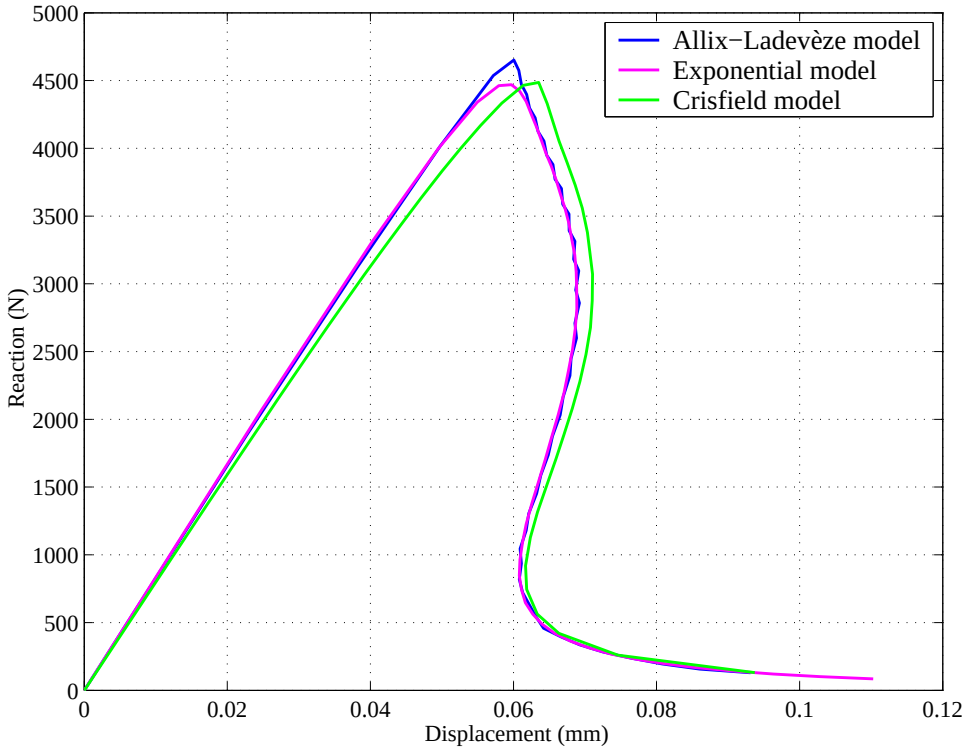

Figure 11: MMT test. Computed load-deflection curves.

As for the compact specimen examined in the second example, a small though appreciable difference is obtained in the computed response for the three models; in particular, the Allix-Ladevèze and exponential models exhibit a slightly stiffer response.

This can again be attributed to the fact that the stiffness of the sample is high enough to put forward the differences between the three interface models, and in particular the differences in the location of the local peak stress, which is indeed attained for a lower value of the relative-displacement for the bi-linear model with respect to the other ones.

4 CLOSURE

It has been presented a comparison between two cohesive-zone models for the analysis of debonding problems.

The first one, developed by Valoroso and Champaney, relies upon a formulation that allows to recover several earlier interface models, and in this work has been implemented with both polynomial and exponential damage laws; the second model studied, originally developed by Crisfield and co-workers and later modified by Alfano and Crisfield, specialises to bi-linear interface relationships for pure-mode cases.

In order to compare the different models, the interface parameters have been chosen in a way to have the same pure-mode undamaged stiffnesses, fracture energy and peak stress for all of them; furthermore, for the mixed-mode case use has been made of two generalized ellipse-like criteria determining damage onset and decohesion propagation.

Numerical simulations have been carried out for several examples referring to both single-mode and mixed-mode situations.

The presented results show that for certain problems the shape of the traction-separation law does produce appreciable differences in the computed global response; in particular, the differences between the load-deflection curves obtained for the three models considered become more evident by increasing the stiffness of the specimen.

Future work will concern a more deep comparison also in terms of stress and strain fields predicted in the vicinity of the process zone, traction profiles along the interface and computational cost of the different models with reference to both 2D and 3D problems.

ACKNOWLEDGEMENTS

This work has been partly carried out within the framework of the activities of the *Laboratoire Lagrange*, an European research group gathering CNR, CNRS, Università di Roma "Tor Vergata", Université de Montpellier II, ENPC, LCPC.

NV acknowledges the Italian National Research Council (CNR) and the Italian Ministry of Education, University and Research (MIUR) for the financial support through the Cofin 2003 research program.

GA acknowledges the financial support of the Italian Ministry of Education, University and Research (MIUR), through the Cofin 2002 research program, and of the Regione Campania, through the research program ex. l. 5, year 2002.

REFERENCES

[1] O. Allix and P. Ladevèze. Interlaminar interface modelling for the prediction of delamination. *Composite Structures*, 22(4):235–242, 1992.

[2] O. Allix and A. Corigliano. Modeling and simulation of crack propagation in mixed-modes interlaminar fracture specimens. *International Journal of Fracture*, 77:111–140, 1996.

[3] G.T. Camacho and M. Ortiz. Computational modelling of impact damage in brittle materials. *International Journal of Solids and Structures*, 33(20–22):2899–2938, 1996.

[4] J.L. Chaboche, R. Girard, and A. Schaff. Numerical analysis of composite systems by using interphase/interface models. *Computational Mechanics*, 20:3–11, 1997.

[5] A. Corigliano. Formulation, identification and use of interface models in the numerical analysis of composite delamination. *International Journal of Solids and Structures*, 30(20):2779–2811, 1993.

[6] A. Corigliano and M. Ricci. Rate-dependent interface models: formulation and numerical applications. *International Journal of Solids and Structures*, 38(4):547–576, 2001.

[7] L. Daudeville and P. Ladevèze. A damage mechanics tool for laminate delamination. *Computers & Structures*, 25:547–555, 1993.

[8] Y. Mi, M.A. Crisfield, G.A.O. Davies, and H.B. Hellweg. Progressive delamination using interface elements. *Journal of Composite Materials*, 32(14):1246–1272, 1998.

[9] A. Needleman. An analysis of tensile decohesion along an interface. *Journal of the Mechanics and Physics of Solids*, 38(3):289–324, 1990.

[10] V. Tvergaard and J.W. Hutchinson. The relation between crack growth resistance and fracture process parameters in elastic-plastic solids. *Journal of the Mechanics and Physics of Solids*, 40(6):1377–1397, 1992.

[11] V. Tvergaard and J.W. Hutchinson. The influence of plasticity on mixed mode interface toughness. *Journal of the Mechanics and Physics of Solids*, 41(6):1119–1135, 1993.

[12] X.P. Xu and A. Needleman. Numerical simulations of fast crack growth in brittle solids. *Journal of the Mechanics and Physics of Solids*, 42:1397–1434, 1994.

[13] G. Alfano and M.A. Crisfield. Solution strategies for the delamination analysis based on a combination of local-control arc-length and line searches. *International Journal for Numerical Methods in Engineering*, 58:999–1048, 2003.

[14] J.R. Reeder. An evaluation of mixed-mode delamination failure criteria. Technical Memorandum 104210, NASA, 1992.

[15] N. Valoroso and L. Champaney. A damage mechanics-based approach for modelling decohesion in adhesively bonded assemblies. 2004. Submitted.

[16] N. Valoroso and L. Champaney. A damage model for simulating decohesion in adhesively bonded assemblies. In P. Neittaanmäki, T. Rossi, K. Majava, and O. Pironneau, editors, *European Congress on Computational Methods in Applied Sciences and Engineering*, Jyväskylä, 2004.

[17] O. Allix, P. Ladevèze, and A. Corigliano. Damage analysis of interlaminar fracture specimens. *Composite Structures*, 31(1):61–74, 1995.

[18] G. Alfano and M.A. Crisfield. Finite element interface models for the delamination analysis of laminated composites: mechanical and computational issues. *International Journal for Numerical Methods in Engineering*, 50(7):1701–1736, 2001.

[19] C. Truesdell and W. Noll. The non-linear field theories of mechanics. In S. Flügge, editor, *Handbuch der Physik Band III/3*, Berlin, 1965. Springer.

[20] G.E. Andrews and R. Roy. *Special functions*. Cambridge University Press, Cambridge, 1999.

[21] CEA, http://www-cast3m.cea.fr/cast3m/. *CAST3M - User Manual*, 2003.

[22] FEA Ltd, Kingston-upon-Thames, UK. *LUSAS - User Manual*, 1999.

[23] G. Alfano. On the influence of the shape of the interface law on the application of cohesive-zone models. 2004. Submitted.

[24] A.J. Russell and K.N. Street. Moisture and temperature effects on the mixed-mode delamination fracture of unidirectional graphite/epoxy. In W.S. Johnson, editor, *Delamination and Debonding of Materials*, ASTM STP 876, pages 349–370, Philadelphia, 1985. American Society for Testing Materials.